Electron mobility in low-temperature $Hg_{1-x}Cd_xTe$ under high-intensity CO_2 laser excitation

F. J. Bartoli, J. R. Meyer, C. A. Hoffman, and R. E. Allen
Naval Research Laboratory, Washington, D.C. 20375
(Received 16 August 1982)

A photo-Hall technique has been employed to determine the dependence of the low-temperature electron mobility in narrow-gap $Hg_{1-x}Cd_xTe$ ($x \approx 0.2$) on optically generated carrier density. Excitation is provided by CO_2 laser pulses of 200-nsec or 25-μsec duration. At low excitation levels the mobility is found to increase due to the neutralization of ionized acceptors by the photoexcited holes. At higher excitation levels the mobility decreases due to electron-hole scattering. Comparison is made to a theory which fully incorporates the Kane band model in treating the scattering of electrons by ionized impurities, photoexcited holes, and compositional disorder. The adaptation of the partial-wave phase-shift method to a nonparabolic band structure is discussed. The treatment of electron-hole scattering incorporates a recently developed theory which accounts in detail for the dynamic dielectric response of the lattice polarizability and free carrier screening. With the use of the random-phase-approximation dielectric constant $\epsilon(q,\omega)$ for arbitrary degeneracy, it is found to be particularly important that the screening by photoexcited holes be treated dynamically. Because the mobility increase at low excitation levels is highly sensitive to the number of acceptors present in the sample, the photo-Hall technique is quite promising as a means of accurately determining compensation densities in narrow-gap $Hg_{1-x}Cd_xTe$.

I. INTRODUCTION

Low-temperature electron mobilities in narrow-gap n-type $Hg_{1-x}Cd_xTe$ have been studied experimentally by a number of previous workers.[1-9] It has been determined that for equilibrium carrier densities, ionized-impurity scattering and compositional-disorder scattering dominate the electron transport below ≈ 40 K. However, a number of additional processes become important if a high-density electron-hole plasma is introduced into the crystal. Here we report a detailed experimental and theoretical investigation of this problem.

The experiment employs a photo-Hall technique to determine the electron mobility as a function of carrier concentration. With the use of laser radiation for the generation of excess carriers, the electron-hole density can be increased by over an order of magnitude. The experiment is carried out at low temperatures ($T \approx 10$ K) where the transport properties are limited by charged-center scattering effects.

The theoretical analysis considers ionized-impurity scattering, electron-hole scattering, and compositional-disorder scattering within the framework of the Kane band model. Charged-center scattering is treated by the partial-wave phase-shift method, employing a form of the Friedel sum rule which accounts for the nonparabolicity of the conduction band. At low excitation levels where ionized-impurity scattering dominates, the scattering by the impurities is made less effective by the additional screening of the excess carriers. It also depends on the extent to which any compensating acceptors are neutralized by photoexcited holes. At sufficiently high excitation levels the electron mobility should be limited primarily by electron-hole scattering. This mechanism is in some ways similar to electron-ion scattering in that both represent interactions with a charged center which is screened by the surrounding dielectric medium. However, there are significant differences due to the mobile nature of the hole scattering center. This problem is considered in detail using a theory which incorporates the dynamics of both lattice polarization and free carrier screening.[10]

An application of photo-Hall techniques to an accurate determination of compensation densities in narrow-gap $Hg_{1-x}Cd_xTe$ is discussed.

II. THEORY

Mobilities for electrons in a nonphotoexcited narrow-gap semiconductor have been calculated by a number of previous investigators.[11-16] Here we outline a theory for the low-temperature mobility of electrons in a photoexcited direct-gap semiconductor. Although application is eventually made to

$Hg_{1-x}Cd_xTe$ with $x \approx 0.2$, the discussion of this section will emphasize the general aspects of the theory. The formulation fully incorporates the Kane band model,[17] which is briefly summarized in Appendix A.

A. Mobility formulation and scattering mechanisms

Because the dominant scattering mechanisms are nearly elastic, we may accurately employ the relaxation time approximation to solve the Boltzmann equation. The mobility is then given by[12]

$$\mu = \frac{e}{3\pi^2\hbar^2 n} \int_0^\infty \left[-\frac{\partial f_0}{\partial E} \right] \tau(E) k^2(E) \frac{dE}{dk}\, dE, \tag{2.1}$$

where n is the electron density, f_0 is the Fermi distribution function, τ is the energy-dependent relaxation time, and the nonparabolic expressions for $k^2(E)$ and dk/dE are given by Eqs. (A2) and (A5) of Appendix A. When several scattering mechanisms must be considered at the same time, the relaxation time can be written

$$\tau(E) = \left[\sum_j \tau_j^{-1}(E) \right]^{-1}, \tag{2.2}$$

where $\tau_j(E)$ is the relaxation time for the jth process acting alone. In photoexcited $Hg_{1-x}Cd_xTe$ at temperatures below about 30 K, the dominant scattering mechanisms are ionized-impurity scattering, electron-hole scattering, and disorder scattering.

1. Ionized-impurity scattering

Electrons may be assumed to interact with ionized impurities via the screened Coulomb potential

$$U(r) = -\frac{Z_I e^2}{\epsilon_0 r} e^{-r/\lambda_s}, \tag{2.3}$$

where Z_I is the impurity charge in units of e, ϵ_0 is the static dielectric constant, and λ_s is the static screening length, which will be discussed below.

In the past, scattering cross sections for the screened Coulomb potential have usually been obtained in the Born approximation. However, more accurate results can be derived using the partial-wave phase-shift method.[18-21] Although an equivalent Hamiltonian formulation[22] can be employed to generalize the partial-wave method to the treatment of a nonparabolic band structure, one can show that it is not, in fact, necessary to use such a theory to find the phase shifts. This is because any electron whose energy is sufficiently small to invalidate the Born approximation is close enough to the bottom of the conduction band to have a nearly parabolic dispersion. It is shown in Appendix B that this is true quite generally for electrons in any of the common direct-gap semiconductors. Results of the more general theory[22] verify that the phase-shift cross sections derived assuming a parabolic band structure can be accurately used in the present nonparabolic calculation. We, therefore, employ recent phase shift results which can be applied to range of the scattering parameters.[21]

The ionized-impurity-scattering relaxation time can be written

$$\tau_I^{-1}(E) = \frac{2\pi N_I Z_I^2 e^4 F_I}{\hbar \epsilon_0^2} \frac{1}{k_e^2} \frac{dk_e}{dE} H_0(E), \tag{2.4}$$

where N_I is the impurity density and H_0 is the phase-shift correction which can be obtained from Ref. 21 (i.e., $H_0 \to 1$ when the Born approximation is valid). The dimensionless screening factor F_I is given by Eq. (3.10) of Ref. 13. In the limit of parabolic bands F_I has the familiar form $F_I \to \ln(b_e+1) - b_e/(b_e+1)$, where $b_e \equiv 4k_e^2\lambda_s^2$. The static screening length λ_{sB}, which is appropriate when the Born approximation is valid, may be obtained from the expression[23]

$$\lambda_{sB}^{-2} = \frac{4\pi e^2}{\epsilon_0} \left[\frac{dn}{dE_{Fn}} + \frac{dp}{dE_{Fp}} \right]. \tag{2.5}$$

Here n and p are the electron and hole densities, E_{Fn} and E_{Fp} are their respective quasi-Fermi energies, and the relation dn/dE_{Fn} is given for nonparabolic bands by Eq. (A9) of Appendix A. When the electrons are degenerate in a narrow-gap semiconductor and $n \approx p$, the hole contribution to the screening is much larger than that of the electrons due to the larger effective mass and smaller Fermi energy.

In the phase-shift formalism, one usually takes the screening length to have the form $\lambda_s \to \lambda_q \lambda_{sB}$, where λ_q is fixed by the requirement that the generalized Friedel sum rule[24] must be satisfied. For parabolic bands the sum rule is

$$Z_I = -\frac{2}{\pi} \sum_{i=e,h,l} q_i \int_0^\infty \left[-\frac{\partial f_0}{\partial E} \right] \times \sum_l (2l+1)\, \delta_l(y_i, b_i)\, dE, \tag{2.6}$$

where the summation i is over the different species of free carriers which can contribute. Here q_i is the charge of carrier type i in units of e, δ_l is the phase shift for the lth partial wave, $b_i \equiv 4k_i^2\lambda_s^2$, and $y_i \equiv \frac{1}{2}ka_{0i}$, where $a_{0i} \equiv \hbar^2\epsilon/m_i q_i Z_I e^2$ (a_{0i} is the

effective Bohr radius if the scattering center is attractive, i.e., $q_i Z_I < 0$). One satisfies the sum rule by adjusting λ_q (and hence b_i) until the two sides of Eq. (2.6) are equal. In Ref. 21, the summation over partial waves is evaluated as a function of y_i and b_i. Results are given in the form

$$\sum_l (2l+1)\,\delta_l(y_i,b_i) = \frac{b_i}{4y_i} S_0(b_i y_i). \quad (2.7)$$

At high energies (specifically when $y_i \gg 1$) the Born approximation is valid and S_0 reduces to unity. It can be shown that whenever $S_0(y_i,b_i) \to 1$ for all i, Eq. (2.6) is satisfied only for $\lambda_q = 1$. That is, $\lambda_s \to \lambda_{sB}$ in this limit, which is why λ_{sB} is referred to above as the Born-approximation screening length.

For the present case we must generalize the Friedel sum rule to include the Kane band structure. Assuming nonparabolic dispersion, the sum rule can be rederived by the same steps discussed in Ref. 21 to yield the following result:

$$Z_I = -\frac{2}{\pi} \sum_{i=e,h,l} q_i \int_0^\infty \left[-\frac{\partial f_0}{\partial E}\right] \left[\frac{b_i}{4y}\right] S_0(b_i,y_i) \left[\frac{2E}{k_i(E)}\frac{dk_i}{dE}\right] dE, \quad (2.8)$$

where the bracketed factor $[(2E/k_i)(dk_i/dE)]$ reduces to unity in the parabolic limit. The integration in Eq. (2.8) is performed over both low E where the Born-approximation invalidity must be accounted for ($S_0 \neq 1$) and high E where for nonparabolic bands the bracketed factor is different from unity. The use of the nonparabolic sum rule Eq. (2.8) enables us to fully incorporate both the Kane band structure and the more accurate scattering cross sections obtained by the partial-wave phase-shift method.

2. *Electron-hole scattering*

Electron-hole scattering is much like electron-ion scattering in that both occur via a Coulomb potential which is screened by a dielectric medium. The main difference is that the ion is stationary, whereas the hole is moving through the crystal with a finite velocity. Although the bare potential is a Coulomb interaction in both cases, the lattice polarization and free carrier screening can be much different due to the frequency dependence of their dielectric response. It has been suggested by a number of authors[13,16] that in treating electron-hole scattering, the high-frequency dielectric constant ϵ_∞ should be employed rather than ϵ_0. It has also been stated[11,14] that the free holes are unable to take part in screening of the electron-hole interactions. We now show that neither of these assertions is accurate[25] when applied to photoexcited plasmas of electrons and holes in $Hg_{1-x}Cd_xTe$.

First, consider the following phenomenological argument, in which we assume that a hole scattering center is moving through the crystal with a velocity v_h. The appropriate value of the dielectric constant to be employed in calculating the transition rate depends on the extent to which the lattice ions contribute to the dielectric polarization. This depends on τ_c, the time scale for variations of the charge density in the vicinity of a given lattice ion, as compared to the lattice response time $\tau_L \approx \omega_{\rm op}^{-1}$, where $\omega_{\rm op}$ is the optical phonon frequency. The time τ_c may be characterized by how long it takes for the hole scattering center to move through some appropriate interaction distance r_0, which is estimated in Appendix D. We thus have $\tau_c \approx r_0/v_h$, where v_h is the hole velocity. When $\tau_c \gg \tau_L$ the lattice can respond and ϵ_0 may be employed. When $\tau_c \ll \tau_L$ the lattice response is too slow and ϵ_∞ is appropriate. For $\tau_c \approx \tau_L$ neither approximation is adequate and the frequency dependence of ϵ must be taken into account.

A similar argument can be made concerning the screening by free electrons and holes. The time τ_i required for carriers of type i to adjust their spatial distribution in response to a change in potential is roughly the time it takes for a particle of average velocity $\bar{v}_i$ to traverse the region of the interaction: $\tau_i \approx r_0/\bar{v}_i$. Comparing τ_i to the time scale for the disturbance, one finds $\tau_c/\tau_i \approx \bar{v}_i/v_h$. Since the relation $\bar{v}_e \gg v_h$ almost always holds, the electrons view the test hole as a nearly static scattering site which they can screen as such. However, with $\bar{v}_h \approx v_h$ the screening by other holes of all but the slowest test holes is at best marginal. These phenomenological conclusions will be verified in the more rigorous treatment which follows.

Having discussed some of the main physical considerations, we now outline the results of a recent theory for dynamic dielectric response to electron-hole interactions.[10] The general approach is to consider the response of a dielectric medium to a potential traveling through that medium with the velocity of the electron-hole center of mass, $\bar{v}_{\rm c.m.}$. One finds after a transformation from crystal coordinates (the rest frame of the medium) to center-of-mass coordinates, that the bare Coulomb potential in momentum space $V(\vec{q}) = 4\pi e^2/q^2$ is modified by a

TABLE I. $Hg_{1-x}Cd_xTe$ material parameters.

E_g	$-0.31 + 1.88x + 5 \times 10^{-4}$ T $(1 - 2x)$	a
E_p	18.5	b
Δ_{so}	1 eV	b
m_h	$0.5m_o$	b
ϵ_0	$20.5 - 15.6x + 5.7x^2$	Fit to data in b
ϵ_∞	$15.2 - 15.6x + 8.2x^2$	Fit to data in b
$\frac{S_1}{S_1+S_2}$	0.95	c
ω_1	2.25×10^{13} sec^{-1}	c
ω_2	2.90×10^{13} sec^{-1}	c
Γ_1, Γ_2	1.50×10^{12} sec^{-1}	c

[a]M. H. Weiler, R. L. Aggarwal, and B. Lax, Phys. Rev. B 16, 3603 (1977).
[b]R. Dornhaus and G. Nimtz, Tracts in Modern Physics 78, 1 (1976).
[c]D. L. Carter, M. A. Kinch, and D. D. Buss, in *The Physics of Semimetals and Narrow Gap Semiconductors*, edited by D. L. Carter and R. T. Bate (Pergamon, Oxford, 1971), p. 273.

frequency-dependent dielectric constant $\epsilon(\vec{q}, \omega)$:

$$U(\vec{q}, \vec{v}_{\text{c.m.}}) = \frac{V(\vec{q})}{\epsilon(\vec{q},\omega)}, \qquad (2.9)$$

where $\omega \equiv \vec{q} \cdot \vec{v}_{\text{c.m.}}$. In the present calculation we restrict our attention to electron scattering by heavy holes, for which $m_h \gg m_e$ and $\vec{v}_{\text{c.m.}} \to \vec{v}_h$. The total dielectric constant $\epsilon(\vec{q}, \omega)$ of the medium is taken to have the form

$$\begin{aligned}\epsilon(\vec{q}, \omega) &= \epsilon_\infty + \epsilon_{\text{lat}}(\omega) + \epsilon_e(\vec{q}, \omega) + \epsilon_h(\vec{q}, \omega) \\ &\equiv \epsilon_R(\vec{q}, \omega) + i\epsilon_I(\vec{q}, \omega), \qquad (2.10)\end{aligned}$$

where ϵ_∞ is the contribution of the rapidly responding core electrons, ϵ_{lat} is due to lattice polarization, and ϵ_e and ϵ_h are the electron and heavy-hole screening contributions, respectively (the light holes have been ignored).

For the lattice contribution we may use the two-mode expression[26]

$$\epsilon_{\text{lat}}(\omega) = \sum_{j=1}^{2} \frac{S_j\omega_j^2}{\omega_j^2 - \omega^2 + i\omega\Gamma_j}, \qquad (2.11)$$

where $S_1+S_2=\epsilon_0-\epsilon_\infty$. The mode strengths S_j, frequencies ω_j, and damping coefficients Γ_j given by Carter, Kinch, and Buss[26] for $Hg_{0.8}Cd_{0.2}Te$ are listed in Table I.

For the free electrons and holes we use the random-phase-approximation dielectric constant[27]

$$\epsilon_i(\vec{q}, \omega) = \frac{4\pi e^2}{q^2} \sum_{\vec{k}} \frac{f_{0i}(\vec{k}) - f_{0i}(\vec{k} + \vec{q})}{E_i(\vec{k} + \vec{q}) - E_i(\vec{k}) - \hbar\omega - \frac{1}{2}i\hbar\Gamma_i}, \qquad (2.12)$$

where to a first approximation the damping coefficient is[28] $\Gamma_i \approx e/m_i\mu_i$ and μ_i is the mobility of carrier type i. Following the conversion of the summation over states in $\vec{k}$ space to a d^3k integral, one finds that both the real and imaginary parts of ϵ_i can be reduced to onefold integrals which must be evaluated numerically unless extreme degeneracy is assumed (see the expressions and discussion in Ref. 10). In the limit $\omega \to 0$, $\Gamma_i \to 0$ and $(\hbar q^2/2m_i n_i)dn_i/dE_{Fi} \ll 1$, Eq. (2.12) can be shown to yield the usual static screening: $\epsilon_e(\vec{q}, \omega) + \epsilon_h(\vec{q},\omega) \to \epsilon_0\lambda_{sB}^{-2}\vec{q}^{\,2}$ and $\epsilon_I \to 0$. Since $\epsilon_{\text{lat}}(\omega \to 0) = \epsilon_0 - \epsilon_\infty$, one obtains in this limit the usual statically screened Coulomb potential [see Eq. (2.9)]: $U \to 4\pi e^2/\epsilon_0(q^2 + \lambda_{sB}^{-2})$, which is just the Fourier transform of Eq. (2.3). In the opposite limit where $\hbar\omega$ is much larger than typical values of $E_i(\vec{k} + \vec{q}) - E_i(\vec{k})$ in the denominator of Eq. (2.12), one obtains that for weak damping the real part of the free carrier component is[29] $\epsilon_{iR}(q, \omega) \to -\omega_{pi}^2/\omega^2$, where ω_{pi} is the plasma frequency ($\omega_{pi}^2 = 4\pi n_i e^2/m_i$). Since ϵ_{iR} is negative in this frequency regime, the real part of the total dielectric constant may vanish when the core electron, lattice, and free carrier contributions are summed. While this does occur, it is shown in Ref. 10 that ϵ_I is usually large in such cases so that resonance behavior is not expected to have a significant effect on the mobility.

We now derive the transition rate due to the electron-hole scattering potential given by Eqs. (2.9)–(2.12). The usual phase-shift method is inapplicable in the present case because the r-space potential obtained from a Fourier transform of

$U(\vec{q}, \vec{v}_{c.m.})$ in Eq. (2.9) is not spherically symmetric. (It has circular symmetry only about the axis defined by $\vec{v}_{c.m.}$). We therefore employ the Born approximation and then incorporate a phase-shift correction as discussed below. The calculation is considerably simpler if we assume the electron-hole interactions to be elastic, since the relaxation time approach cannot be used unless this approximation is made. It is shown in Appendix C that the assumption of elasticity is valid whenever $m_h \gg m_e$ and the electron Fermi level is not too great. For $Hg_{0.8}Cd_{0.2}Te$ it is appropriate at any photoexcited carrier density below about 10^{17} cm^{-3}.

In the Born approximation, the transition rate for electrons of wave vector $\vec{k}_e$ scattering to the state $\vec{k}_e'$ is

$$W_{eh}(\vec{k}_e \rightarrow \vec{k}_e') = 2\left[\frac{m_h}{2\pi\hbar}\right]^3 \int d^3v_h f_0(v_h)\,[1 - f_0(v_h')] \left[\frac{2\pi}{\hbar}\right] \delta(E_e + E_h - E_e' - E_h') \times |\, U(\vec{q}, \omega = \vec{q}\cdot\vec{v}_h)\,|^2, \tag{2.13}$$

where $\vec{q} = \vec{k}_e - \vec{k}_e'$, $|\vec{v}_h'| = |\vec{v}_h + \hbar\vec{q}/m_h| \rightarrow |\vec{v}_h|$ (assuming elasticity) and

$$|\,U(\vec{q},\omega)\,|^2 \rightarrow \left[\frac{4\pi e^2}{q^2}\right]^2 \left[\frac{1}{\epsilon_R^2(\vec{q},\omega) + \epsilon_I^2(\vec{q},\omega)}\right]. \tag{2.14}$$

The integration in Eq. (2.13) is over the Fermi distribution of holes from which scattering can occur.

Of the three integrals in Eq. (2.13), the azimuthal angle integral $d\phi_h$ is trivial. A second integral can be performed if we first change coordinates from v_h to $\omega = qv_h\,|u'|$, where $u' \equiv \cos\theta_h$ and θ_h is the angle between $\vec{v}_h$ and $\vec{q}$. One obtains

$$W_{eh}(\vec{q}) = \frac{16\pi e^4 m_h^3}{\hbar^4 q^7}\,\delta(E_e - E_e') \int_{-1}^{1} \frac{du'}{|u'|^3} \int_0^\infty \omega^2 d\omega\, \frac{f_0(E_h = m_h\omega^2/2q^2u'^2)\,[1 - f_0(E_h)]}{\epsilon_R^2(\vec{q},\omega) + \epsilon_I^2(\vec{q},\omega)}. \tag{2.15}$$

Since the du' integral is even, we may take $\int_{-1}^{1} du' \rightarrow 2\int_0^1 du'$. After changing variables from u' to $z = m_h\omega^2/2q^2u'^2k_BT$ one can integrate to obtain

$$W_{eh}(q) = \frac{32\pi e^4 k_B T m_h^2}{\hbar^4 q^5}\,\delta(E_e - E_e') \int_0^\infty \frac{d\omega}{\epsilon_R^2(q,\omega) + \epsilon_I^2(q,\omega)}\, \frac{1}{e^{m_h\omega^2/2q^2k_BT - E_{Fp}/k_BT} + 1}. \tag{2.16}$$

Since the last factor inside the integral of Eq. (2.16) is simply $f_0(v_h')$ if $v_h' \rightarrow \omega/q$, we rewrite Eq. (2.16) in the form

$$W_{eh}(q) = \frac{32\pi e^4 k_B T m_h^2}{\hbar^4 q^4}\,\delta(E_e - E_e') \int_0^\infty \frac{f_0(v_h')dv_h'}{\epsilon_R^2(q,\omega = qv_h') + \epsilon_I^2(q,\omega)}. \tag{2.17}$$

The electron-hole-scattering relaxation time can now be evaluated from

$$\tau_{eh}^{-1}(E_e) = \frac{1}{(2\pi)^3} \int d^3k_e'\, W_{eh}(\vec{k}_e \rightarrow \vec{k}_e')\,(1 - \cos\theta) O(\cos\theta), \tag{2.18}$$

where θ is the angle between $\vec{k}_e$ and $\vec{k}_e'$. The dimensionless wave-function admixture factor $O(\cos\theta)$ is usually on the order of unity and is defined in the Appendix of Ref. 15. After substitution of W_{eh} and evaluation of two of the three integrals in Eq. (2.18), one obtains

$$\tau_{eh}^{-1}(E_e) = \frac{2e^4 k_B T m_h^2}{\pi\hbar^4}\, k_e^{-2} \frac{dk_e}{dE_e}\, H_0(E_e) \int_0^\pi \frac{O(\cos\theta)\sin\theta\, d\theta}{1 - \cos\theta} \int_0^\infty \frac{f_0(v_h')dv_h'}{\epsilon_R^2(q,\omega = qv_h') + \epsilon_I^2(q,\omega)}, \tag{2.19}$$

where the relation $q^2 = 2k_e^2(1 - \cos\theta)$ has been used. We have inserted a phase-shift correction factor H_0 which can be calculated in the manner discussed above for ionized impurities. Although the values for H_0 given in Ref. 21 were obtained assuming static screening, the error introduced should not be large since the Born approximation is nearly valid under high photoexcitation conditions where electron-hole scattering is important.

Equation (2.19) represents our final result for the relaxation time due to electron-hole scattering. It is instructive to evaluate this expression in the static limit, i.e., for $\epsilon(q,\omega) \to \epsilon_0(1+\lambda_{sB}^{-2}\bar{q}^{2})$. The dielectric constant can then be removed from the dv_h integral, which can be written

$$\frac{m_h^2 k_B T}{\pi^2 \hbar^3} \int_0^\infty f_0 dv_h' = -\frac{k_B T}{\pi^2} \int_0^\infty \frac{\partial f_0}{\partial E} k_h^2 dk_h$$

$$= \frac{1}{\pi^2} \int_0^\infty f_0(1-f_0) k_h^2 dk_h$$

$$\equiv p', \qquad (2.20)$$

where comparison with Eq. (A9) of Appendix A gives that $p' = k_B T dp/dE_{Fp}$. Substitution into Eq. (2.19) yields

$$\tau_{eh}^{-1}\,(\text{static}) = \frac{2\pi p' e^4 F_I}{\hbar \epsilon_0^2} k_e^{-2} \frac{dk_e}{dE} H_0. \qquad (2.21)$$

The static electron-hole relaxation time Eq. (2.21) is therefore completely analagous to the ionized-impurity-scattering result Eq. (2.4) except that the effective density of scattering centers is p' rather than the actual hole density p. In the nondegenerate limit, the factor $(1-f_0)$ can be replaced by unity and $p' \to p$. However, when the holes are degenerate the effective density of scattering centers is much less than the hole density because in most of the possible interactions the final hole state is already occupied. The same qualitative considerations apply to the more general dynamic result Eq. (2.19), although there one does not obtain an easily recognizable "effective density of scattering centers."

Having developed both static and dynamic expressions for the electron-hole relaxation time, we are now in a position to predict quantitatively under what conditions the dynamic effects are important. From Eq. (2.19) we see that the dielectric constant $\epsilon(q,\omega)$ is evaluated at $\omega = qv_h'$. It is shown in Appendix D that the dominant contributions of the integral over θ occurs for $q \approx q_0$, where an expression for q_0 is given by Eq. (D2). Also discussed in Appendix D is the length $r_0 \approx q_0^{-1}$ which characterizes a typical interaction distance. The frequencies of interest are thus of order $\omega_e \approx \bar{v}_h/r_0$, where $\bar{v}_h$ is an appropriate hole velocity.[30] This is in agreement with the conclusion obtained phenomenologically at the beginning of this section that the relevant time scale is $\tau_c \approx \omega_c^{-1} \approx r_0/\bar{v}_h$.

We now define $\epsilon'(\omega)$ to be the sum of the core electron and lattice ion contributions to the dielectric constant. We also define an "effective" value: $\epsilon'_{\text{eff}} \equiv \epsilon_0\{\tau_{eh}[\epsilon_{\text{lat}} = \epsilon_{\text{lat}}(\omega)]/\tau_{eh}[\epsilon_{\text{lat}} = \epsilon_{\text{lat}}(\omega = 0)]\}^{1/2}$. This is approximately that constant value of ϵ' which would give the same relaxation time as that obtained from the general dynamic formulation represented by Eq. (2.19). In Fig. 1, ϵ'_{eff} is plotted as a function of carrier density for $Hg_{0.8}Cd_{0.2}Te$ at 10 K with $n = p$. The shape of the curve is easily understood if we roughly estimate $\epsilon'_{\text{eff}} \approx \epsilon_\infty + \epsilon_{\text{lat}}(\omega_c)$, where $\epsilon_{\text{lat}}(\omega)$ is given by Eq. (2.11). At low carrier densities, $\bar{v}_h$ may be taken as the nondegenerate thermal velocity, which is quite low. Since ω_c is proportional to $\bar{v}_h$, we find that the frequencies of interest are much lower than the frequencies ω_j of the phonon modes. From Eq. (2.11), this implies that the frequency dependence of ϵ_{lat} can be ignored and we obtain $\epsilon'_{\text{eff}} \approx \epsilon_0$. However, for $n \gtrsim 10^{17}$ cm^{-3} the holes begin to become degenerate and the typical velocities increase with carrier density. As ω_c becomes larger, ϵ'_{eff} increases above ϵ_0 before dropping toward ϵ_∞. This is also expected from the form of Eq. (2.11), although the resonance behavior near $\omega_c \approx \omega_j$ has been broadened because Eq. (2.17) contains an integral over ω rather than the discrete value $\omega = \omega_c$. These results illustrate that in treating electron-hole scattering, dynamic polarization effects should be taken into account, and that it is often incorrect to approximate ϵ'_{eff} by ϵ_∞ as is suggested in Refs. 13 and 16.

Dynamic free carrier screening effects are important when $\hbar\omega$ in the denominator of Eq. (2.12) is

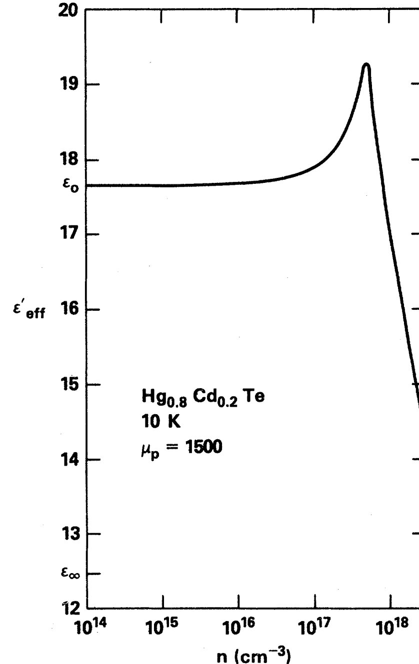

FIG. 1. Effective dielectric constant excluding free carrier screening, plotted as a function of carrier density for $n = p$.

comparable to or larger than $E_i(\vec{k}+\vec{q})-E_i(\vec{k}) \approx \hbar k_i q/m_i$. If we substitute $\omega \approx q\bar{v}_h$ and $\hbar k_i/m_i \to \bar{v}_i$, we find that the static limit is appropriate only when $\bar{v}_h \ll \bar{v}_i$. While the inequality easily holds for electrons, it is necessarily violated for holes. It is clear that while free holes do contribute to the screening of electron-hole interactions, their contribution is never as great as it is in the screening of static potentials. This result can be quantified if we define an "effective" hole screening contribution in the following way. The static expression for the free carrier contribution to the dielectric constant is $\epsilon_i = \epsilon_0 \lambda_{sBi}^{-2} q^{-2}$, where $\lambda_{sBi}^{-2} = (4\pi e^2/\epsilon_0) dn_i/dE_{Fi}$ from Eq. (2.5). If we calculate τ_{eh} from Eq. (2.19) using this static form for electrons but the dynamic expression Eq. (2.12) for holes, an "effective" hole contribution to the screening can be defined as the $\lambda_{sBh}^{-2}(\text{eff})$ which gives the same relaxation time if the holes are also assumed to screen statically. Figure 2 shows a plot of $\lambda_{sBh}^{-2}(\text{eff})/\lambda_{sBh}^{-2}$ vs carrier density for various values of hole mobility assuming the same conditions considered in Fig. 1. Note that in the low damping case (high hole mobilities), the hole screening is approximately 50% effective over the entire range of carrier densities. However, the figure also shows that $\lambda_{sB}^{-2}(\text{eff})$ can be considerably smaller for lower hole mobilities in the range of values observed experimentally.[31–33] This is due to the damping factor Γ_i in Eq. (2.12), which it can be shown becomes important when $\Gamma_i \gtrsim q_0 \bar{v}_i$. Since q_0 is larger at high carrier densities due to the larger electron Fermi energy, the damping is less effective there.

3. Disorder scattering

Electrons in any mixed crystal $A_{1-x}B_xC$ do not perceive a perfect lattice due to short-range compositional disorder.[34] Consequently, disorder scattering has an effect on the electron mobility. In a calculation which incorporates the Kane band model, Kossut has calculated the relaxation time for this process[35]

$$\tau_{\text{DO}}^{-1}(E) = \frac{N_{AB} x(1-x) V^2 F_{\text{DO}}}{\pi \hbar} k_e^2 \frac{dk_e}{dE}, \qquad (2.22)$$

where x is the composition, N_{AB} is the number of C atoms per unit volume, V is a matrix element, and F_{DO} is a dimensionless quantity on the order of unity which contains other matrix elements. [See Eq. (26) of Ref. 35.] For $Hg_{1-x}Cd_xTe$ we have used the values suggested in Ref. 35 for the matrix elements.

Under photoexcitation, τ_{DO}^{-1} increases with n_e due to the factor $k_e^2 dk_e/dE$ which increases with electron Fermi energy. By comparison, τ_I^{-1} for ionized impurities decreases with n_e and τ_{eh}^{-1} for electron-hole scattering increases by no more than[36] $k_e dk_e/dE$. Disorder scattering therefore has a much greater effect on the mobility at high excitation levels.

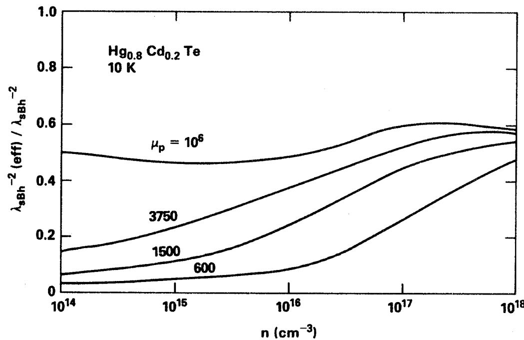

FIG. 2. Ratio of the effective dynamic hole screening to full static screening, plotted as a function of carrier density for $n = p$.

B. Compensation and effects of photoexcitation

The formalism presented above for ionized-impurity and electron-hole scattering may be applied to either compensated or uncompensated narrow-gap semiconductors. However, in order to calculate the relaxation times for these mechanisms, explicit expressions for the electron, hole, and ionized-impurity densities are still required. Assuming a monovalent donor merged with the conduction band, the free electron and hole densities in uncompensated material can be written: $n = N_D + n_e$ and $p \approx p_e = n_e$, where n_e and p_e are the photoexcited electron and hole densities and N_D is the donor density. Since electrons are scattered primarily by impurities and holes at low temperatures, the electron density is approximately equal to the density of scattering centers. However, in compensated material this is no longer the case. If one assumes a single type of divalent acceptor,[37] the electron density is given by

$$n = N_D - 2N_A + n_e, \qquad (2.23)$$

where N_A is the acceptor density. For compensated material one also no longer has $p_e = n_e$ in general, since holes can be captured by the acceptors, thereby reducing their ionization state. The free hole density may therefore be written

$$p = n_e - N_A^{(-1)} - 2N_A^{(0)}, \qquad (2.24)$$

where $N_A^{(-Z)}$ represents the density of acceptors with charge $-Z$ and $N_A = N_A^{(-2)} + N_A^{(-1)} + N_A^{(0)}$. Since the acceptors are all doubly negative in the absence of photoexcitation, $N_A^{(-1)}$ and $N_A^{(0)}$

represent the density of ions which have captured one and two holes, respectively.

We now examine qualitatively the effects of photoexcitation on the electron mobility in compensated material. At low excitation levels the photoexcited holes are captured by acceptors,[9] thereby decreasing the charge states from -2 to -1. At the same time, the larger electron density contributes to greater screening of the Coulomb interactions between the electrons and ions. Since a change in acceptor charge from -2 to -1 reduces the scattering cross section by approximately a factor of 4 [see Eq. (2.4)], one expects a pronounced increase in the electron mobility at modest excitation levels for any material which is at least moderately compensated. As the photoexcitation level is increased, the $Z=-2$ acceptors are converted to $Z=-1$ and some of these are then neutralized. The mobility continues to increase in this region, since it can be shown that the cross sections for scattering by neutral acceptors are at least two orders of magnitude smaller than those for ionized acceptors.[38] If the photoexcitation level is increased further, free holes will eventually begin to accumulate and act as scattering centers. Because of screening by the free holes, the electron mobility does not necessarily decrease immediately as soon as $n_e \geq 2N_A$. However, at sufficiently high carrier densities a decrease due to electron-hole scattering is generally predicted.

In calculating the electron mobility from the relaxation time expressions Eq. (2.4) and (2.19), H_0 must be determined and the Friedel sum rule must be satisfied separately for donors, singly changed accepters, and doubly charged acceptors, as well as for the hole scattering centers in electron-hole scattering. The problem is much more difficult if multiple scattering by more than one charged center at a time must be included. This effect has been considered,[39] but is not expected to be important under most conditions achieved in the present experiment.

When the acceptor population has a multiplicity of charge states, there will be an additional contribution to the screening due to the fact that an acceptor near a positive test charge (for example) will on the average have a higher negative charge than one far away. This is similar to the additional screening by bound electrons which was discussed by Brooks[40] for a system containing both ionized and neutral donors. For a system of acceptors with two charge states $N_A^{(1)}$ and $N_A^{(2)}$ one should add to λ_{sB}^{-2} in Eq. (2.5):

$$\lambda_{sB}^{-2}\,(\text{bound holes}) = \frac{4\pi e^2}{\epsilon_0 k_B T}\,\frac{N_A^{(1)}N_A^{(2)}}{N_A^{(1)}+N_A^{(2)}}. \quad (2.25)$$

Under steady-state excitation conditions, the number of acceptors in each of the charge states will depend on the relations between the electron and hole capture cross sections characteristic of each state. We define $\sigma_i^{(-Z)}$ as the cross section for capture of a carrier of type i by acceptors in the charge state $(-Z)$. Photoexcited holes are captured quite readily by the $Z=-2$ acceptors because of the strong Coulomb attraction. On the other hand, electron capture by $Z=-1$ acceptors is highly improbable (i.e., $G_2 \equiv \sigma_n^{(-1)}/\sigma_p^{(-2)} \ll 1$) because of the Coulomb repulsion. This relation implies that in the steady state, very few holes will remain free as long as doubly charged acceptors are present. One also expects that $G_1 \equiv \sigma_n^{(0)}/\sigma_p^{(-1)} \lesssim 1$ since the capture of electrons by neutral acceptors takes place only through a dipole interaction, while the holes interact with the singly charged acceptors through a Coulomb attraction. The neutralization of $Z=-1$ acceptors can be described by the steady-state rate equation for neutral acceptors. By detailed balance one has $nN_A^{(0)}\sigma_n^{(0)} \approx pN_A^{(-1)}\sigma_p^{(-1)}$. For high densities where $n \approx p$, $N_A^{(0)}/N_A^{(-1)} \approx G_1^{-1} \gtrsim 1$, i.e., over half of the $Z=-1$ acceptors are neutralized. For lower excitation levels where $n \gg p$, $N_A^{(0)}/N_A^{(-1)} = (p/n)G_1^{-1}$ which can be appreciably smaller than the high density limit. Although the relevant cross sections have not been determined for divalent acceptors in $Hg_{1-x}Cd_xTe$, both theoretical estimates[41] and data on divalent acceptors in other materials[42] indicate that these general considerations should hold.

III. EXPERIMENTAL APPARATUS AND RESULTS

Photo-Hall and photoconductivity measurements have been performed at 10 K on several n-type $Hg_{1-x}Cd_xTe$ samples with a nominal composition of $x \approx 0.2$. The electron mobility has been determined as a function of carrier density, using CO_2 laser excitation in order to achieve a wide range of electron and hole densities. The experimental configuration employed is illustrated in Fig. 3. The sample was mounted in a variable temperature refrigerator and was situated between the pole pieces of an electromagnet which provided a uniform magnetic field. The laser beam was directed through an aperture in one pole piece of the magnet and focused onto the sample. To insure uniform sample irradiation, the focused spot size was large compared to the sample. Carriers were generated in the sample by interband single-photon absorption of the laser radiation which was pulsed in order to avoid sample heating. The photo-Hall and photoconductivity measurements were made using a high-speed Tektronix R7912 transient digitizer which was inter-

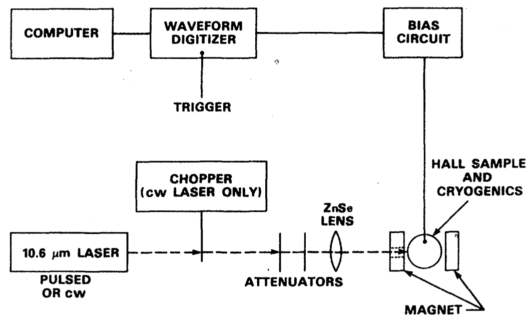

FIG. 3. Experimental configuration.

faced to a PDP 11/03 minicomputer for immediate data storage and processing.

Measurements are reported for three $Hg_{1-x}Cd_xTe$ samples. Samples 1A and 1B are from the same slice of $x = 0.196$ Cominco material, which was processed by Santa Barbara Research Center in a Van der Pauw configuration with dimensions $0.5 \times 0.5 \times 0.1$ mm^3. Sample 2 is a Hall bar $12.6 \times 1.6 \times 0.09$ mm^3 with lateral contacts 2.9 mm on either side of center along the long dimension of the bar. This sample is from $x = 0.215$ material grown and processed by Honeywell, Inc. The values of x given for these samples are believed to be accurate to within ± 0.005. All samples are mounted on sapphire substrates which are bonded to a copper disk in direct contact with the cold finger of an Air Products closed-cycle helium refrigerator. The sample is surrounded by a metal cold shield maintained at 60 K. Optical access is provided by an aperture in the cold shield providing a 60° full-angle field of view and by a BaF_2 window in the external vacuum shroud. A temperature-sensing diode together with a PAR Corporation temperature controller are used for temperature regulation.

Samples 1A and 1B were illuminated by an externally shuttered 50-W cw CO_2 laser, providing 25-μsec flat-top pulses with rise and fall times less than 1 μsec at a repetition rate of 1 Hz. Since the pulse duration is long compared to carrier relaxation and recombination times, one obtains steady-state values of μ and n which can be compared with theoretical calculations based on steady-state optical excitation. The 25-μsec pulse was obtained by focusing the laser beam through a small hole in an 8-in. diam aluminum disk rotating at 100 Hz and recollimating the laser beam after it passed through the shutter. The laser power supply was electrically triggered and synchronized with the shutter to produce at the sample one pulse every second. With this low duty cycle, increases in n by over an order of magnitude were obtained for samples 1A and 1B without appreciable sample heating. For sample 2, however, the larger sample size made it difficult to generate sufficient carrier densities and still maintain uniform irradiation using the 50-W cw laser. To supplement the cw laser source data on sample 2, measurements were also performed employing excitation by 200-nsec pulses from a transversely excited atmosphere CO_2 laser with a 1-Hz repetition rate. The mobility and carrier density were measured as a function of time during and after the laser pulse. To eliminate transient effects, only data taken at least 200 nsec after the laser pulse was used. This portion of the photoexcited electron decay is assumed to yield steady-state values for μ as a function of n. Mobilities obtained using both laser sources are in agreement.

Both CO_2 lasers, operating on the P(20) line with $\lambda = 10.6$ μm, contained intracavity apertures to restrict laser oscillation to the TEM_{100} transverse mode. The optics were adjusted to maintain a transverse Gaussian intensity profile and to yield a spot size large compared to the sample. Variations in intensity, and hence in carrier density, were achieved through the use of variable attenuators consisting of CaF_2 disks of various thicknesses and Ge with reflective coatings. The laser spot intensity profile was measured by substituting a scanning pinhole and detector assembly in place of the sample.

Photo-Hall and photoconductivity voltage traces were obtained and averaged over all possible combinations of bias current polarity, magnetic field polarity and sample contact pairings. In this way any spurious voltages, e.g., associated with sample asymmetry, cancel out leaving the true photo-Hall and photoconductivity signals. An increased signal-to-noise ratio was obtained by averaging signals over many laser pulses for each polarity of bias current and magnetic field, and for each electrical contact configuration. Monitoring of the laser pulse shape and energy throughout the experiments verified that pulse-to-pulse repeatability was usually better than 5%. Data from pulses falling outside of the 5% limit were automatically eliminated by a pulse selection routine in the control software.

Experimental data for the three samples at 10 K are presented in Figs. 4 and 5, which show the measured mobility as a function of carrier density. At low excitation levels the mobility increases due to acceptor neutralization. This effect is much more pronounced in sample 2, which is more compensated. At higher excitation levels the mobility decreases, primarily because of electron-hole scattering. Data for excitation levels high enough to cause sample heating are not included in the figures. While slight carrier heating may occur due to free carrier absorption, it is estimated that the effect on the electron mobility is less than 10%. The data in

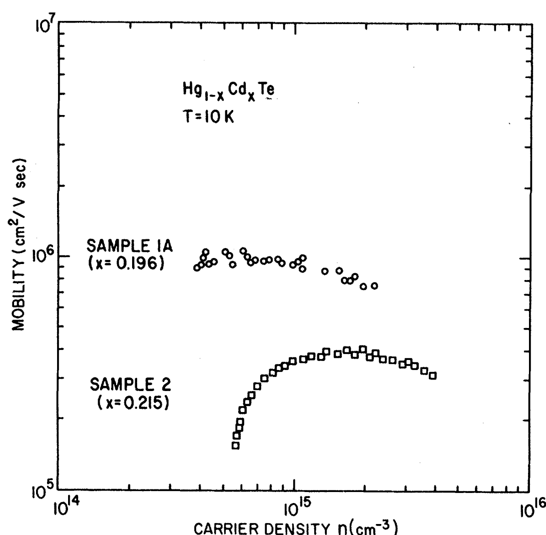

FIG. 4. Raw experimental data for samples 1A and 2.

Figs. 4 and 5 must be corrected for carrier density variation with sample depth, since the laser radiation is absorbed within the first several micrometers of the surface, and the carrier diffusion length is less than the sample thickness. Following the approach of Petritz[43] the sample is treated as two homogeneous layers parallel to the current flow. The thickness of the front layer is determined by the ambipolar diffusion. The front layer is assumed to have a uniform photoexcited carrier density while the back layer retains the dark value n. This correction primarily affects n, while mobility values are only slightly modified. The ambipolar diffusion length can be obtained from the relations $L_D = (D_a\tau)^{1/2}$ and[44]

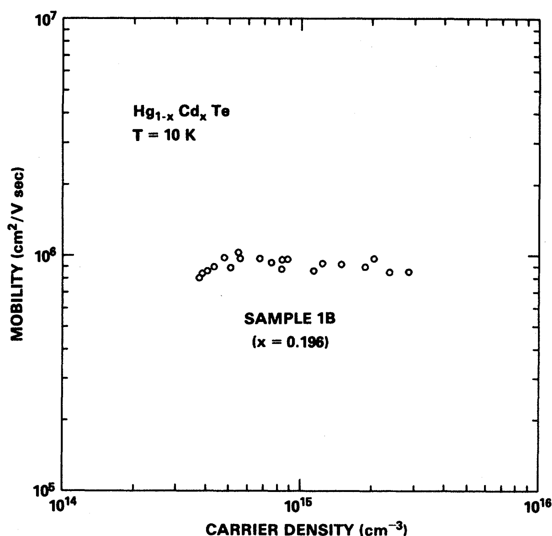

FIG. 5. Raw experimental data for sample 1B.

$$D_a = \frac{np\mu_n\mu_p}{e(n\mu_n + p\mu_p)} \times \left[\left[\frac{dn}{dE_{Fn}} \right]^{-1} + \left[\frac{dp}{dE_{Fp}} \right]^{-1} \right] . \quad (3.1)$$

Evaluating Eq. (3.1) for $\tau \approx 1\ \mu$sec, $\mu_p \approx 1000$ cm²/V sec, and $\mu_n \gg \mu_p$, one obtains L_D on the order of 20 μm with some variation with electron and hole density. In the corrected data shown below in Figs. 6 to 10, $L_D = 20\ \mu$m is assumed.

IV. DISCUSSION

Before making a detailed comparison between theory and the reduced experimental data, we discuss the effect of varying certain parameters which appear in the theory, but which are not presently well known. These are $G_1 \equiv \sigma_n^{(0)}/\sigma_p^{(-1)}$ and the hole mobility μ_p.

For the somewhat compensated sample 2, Fig. 6 shows the effect of varying G_1 between 0.01 and 1.0. Since $N_A^{(-1)} \approx G_1 N_A^{(0)}$ at high excitation levels where $n \approx p$, a larger G_1 tends to lower the mobility because the ionized acceptors scatter more effectively than neutral acceptors. The electron mobility is insensitive to G_1 at very low excitation levels, since there almost all of the photoexcited holes go into converting doubly charged acceptors to singly charged acceptors. It is also insensitive to G at very high excitation levels because electron-hole scattering dominates the scattering in that regime. However, at intermediate excitation levels, the choice of G_1 can affect the calculated mobility by as much as

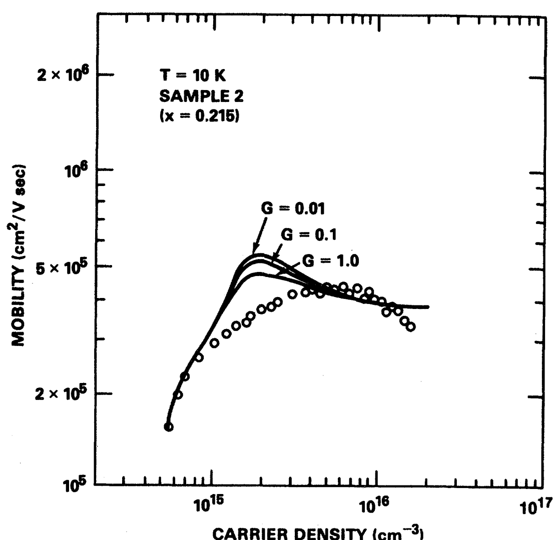

FIG. 6. Reduced experimental data for sample 2 and dependence of theoretical mobility on $G_1 \equiv \sigma_n^{(0)}/\sigma_p^{(-1)}$.

20%. Since the value of G_1 has not been experimentally determined for HgCdTe, we use for convenience the value $G_1 \approx 1.0$ in the following calculations. The mobilities calculated for the less compensated samples 1A and 1B are naturally less sensitive to the choice of G_1.

At high excitation levels, the electron mobility depends on the effectiveness of the dynamic hole screening, and is therefore sensitive to the hole mobility μ_p. (This was discussed in connection with Fig. 2 above.) Hole-mobility measurements on non-photoexcited p-type HgCdTe at temperatures below 77 K are somewhat fragmentary. For doping levels larger than 10^{15} cm^{-3}, mobilities between several hundred and 1000 cm^2/V sec have been reported.[31,32] At 10 K, a value as large as $\mu_p \approx 3000$ has been observed under conditions where most of the acceptors have been neutralized by freezeout of the holes.[33] Under photoexcitation conditions, one expects the mobility to be somewhat higher for a given density of impurities due to screening by excess electrons and holes. An accurate calculation of the hole mobility is difficult, however, because of uncertainties regarding the effects of disorder scattering. If one employs the usual Brooks calculation[34] [the parabolic analog of the formulation discussed in Sec. II A 3], one obtains a disorder-limited mobility of less than 200 cm^2/V sec at any temperature above 10 K. Since this is clearly inconsistent with the experimental data, the Brooks theory appears to work quite poorly in the case of p-type HgCdTe. In the absence of a reliable theory, it is difficult to estimate even the order of magnitude of the disorder-scattering mobility. On the other hand, if disorder scattering is ignored, obtains a calculated low-temperature hole mobility in excess of 10^4 cm^2/V sec for the impurity concentrations of present interest. Since disorder scattering for holes is expected to be relatively insensitive to the levels of doping and photoexcitation while the scattering due to ionized impurities depends strongly on these parameters, it is difficult to estimate even roughly how μ_p should vary with N_D, N_A, n, and p. Figure 7 shows the variation of the calculated electron mobility of sample 1A with μ_p for the values $\mu_p = 600$, 1500, and 3750 cm^2/V sec. Also shown is the reduced experimental data. It can be seen that the shape and magnitude of the experimental mobility is well reproduced if we assume $\mu_p \approx 1500$ cm^2/V sec. In the figures which follow we employ that value for samples 1A and 1B and 1000 cm^2/V sec for sample 2. A somewhat lower value seems appropriate for sample 2 since a greater density of impurities is present.

For the values of G_1 and μ_p stated above, Figs. 8–10 show calculated electron mobilities for all

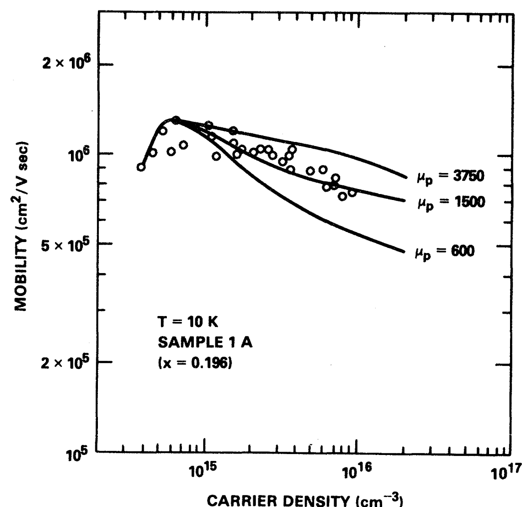

FIG. 7. Reduced experimental data for sample 1A and dependence of theoretical electron mobility on hole mobility.

three samples as a function of excitation level, along with the reduced experimental data. In each figure the three theoretical curves correspond to (1) static screening of electron-hole interactions, (2) dynamic screening of electron-hole interactions, and (3) neglect of hole screening in the electron-hole interactions. The first substantially overestimates the electron mobility for all three samples, while the third underestimates it at most carrier densities. On the other hand, the more general theory for dynamic screening tends to give better agreement at high excitation levels where electron-hole scattering dominates the mobility. At low excitation levels the compensation is used as a fitting parameter. We

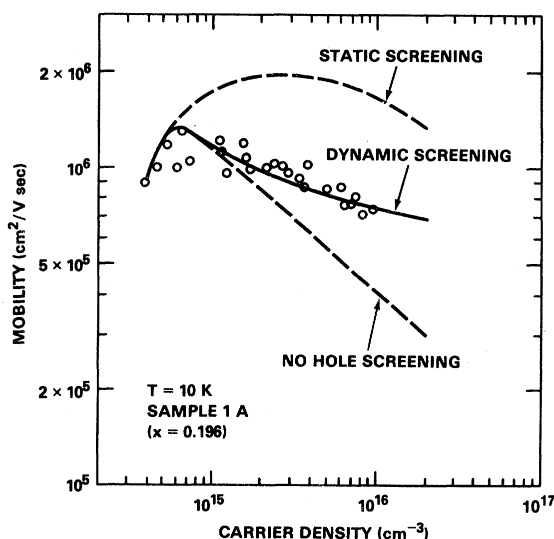

FIG. 8. Theoretical and reduced experimental mobilities vs electron density for sample 1A.

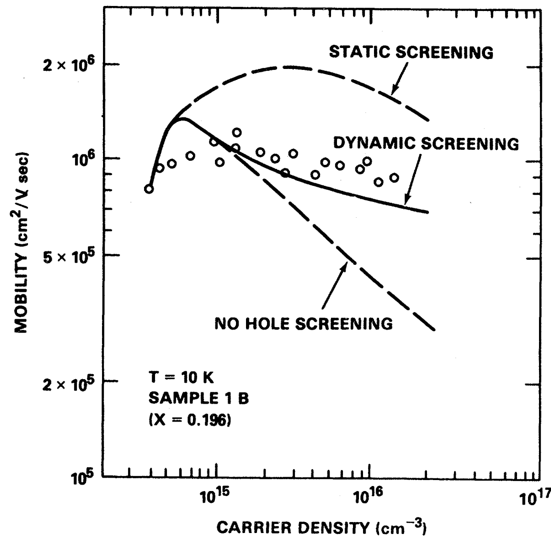

FIG. 9. Theoretical and reduced experimental mobilities vs electron density for sample 1B.

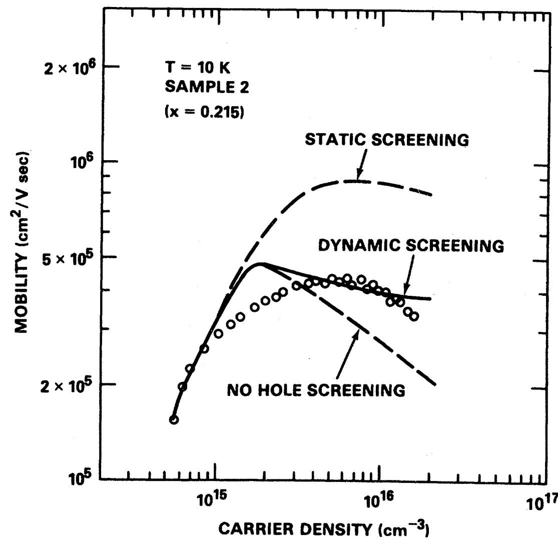

Fig. 10. Theoretical and reduced experimental mobilities vs electron density for sample 2.

find $N_D \approx 4.7 \times 10^{14}$ cm^{-3} and $N_A \approx 4.3 \times 10^{13}$ cm^{-3} for sample 1A, $N_D \approx 4.9 \times 10^{14}$ cm^{-3} and $N_A \approx 5.6 \times 10^{13}$ cm^{-3} for sample 1B, and $N_D \approx 1.6 \times 10^{15}$ cm^{-3} and $N_A \approx 5.4 \times 10^{14}$ cm^{-3} for sample 2.

It is evident from Figs. 8–10 that dynamic response effects are quite important, due primarily to the reduced effectiveness of the hole screening (see Fig. 2). Figure 1 shows that the effective dielectric constant $\epsilon'_{\text{eff}} = \epsilon_\infty + \epsilon_{\text{lat}}$ does not vary significantly from ϵ_0 at $n < 10^{17}$ cm^{-3} because the frequencies of interest [see Eq. (2.19)] are much lower than the phonon mode frequencies in Eq. (2.11). Our conclusion that $\epsilon'_{\text{eff}} \approx \epsilon_0$ differs with previous suggestions that $\epsilon'_{\text{eff}} \approx \epsilon_\infty$.

While the ionized impurity and electron-hole relaxation times increase with electron energy, that for disorder-scattering decreases. Disorder scattering therefore has a greater effect on the mobility of high excitation levels where the electron Fermi energy is high. For example, using Kossut's formulation the inclusion of disorder scattering decreases the mobility of sample 2 by only 2% in the absence of photoexcitation, but by more than 25% at $n = 2 \times 10^{16}$ cm^{-3}.

The lack of theoretical and experimental agreement concerning the shape and location of the mobility peak is probably due to the approximate "two-layer" data reduction technique employed. In a future work, the carrier density versus depth profile will be analyzed in detail to develop a more accurate method of data reduction. Alternatively, one could employ two-photon absorption or less strongly absorbed one-photon excitation to produce highly uniform carrier densities.

It should be noted that uncertainties on the order of ± 0.005 in the composition x, and hence in uncertainties in the band gap and effective mass, can influence the calculated mobilities. Since the high density mobility is dependent only on x and not on the doping level of a particular sample, it should eventually be possible to use the high density data to "calibrate" the composition. The resulting x could then be used in analyzing the data at lower excitation levels where the mobility is sensitive to the impurity concentrations. The principle uncertainty in the present theoretical treatment for high excitation levels is in assigning the appropriate hole mobility for the damping factor in the hole screening term.

V. CONCLUSIONS

Photo-Hall and photoconductivity measurements have been performed on n-type $Hg_{1-x}Cd_xTe$ ($x \approx 0.2$) at 10 K. Electron mobilities have been determined for a wide range of excess electron and hole densities, where CO_2 laser radiation is used as the source of optical excitation. At low excitation levels, the mobility increases primarily due to the neutralization of ionized acceptors by photoexcited holes. With increasing excitation, the mobility passes through a peak and then decreases due to the effects of electron-hole scattering.

Experimental results were compared with a theory for electron mobilities in optically excited narrow-gap semiconductors. The partial-wave phase-shift method was employed in the calculation of ionized-impurity and electron-hole scattering cross sections. Compositional disorder scattering was also considered. In treating electron-hole scattering, it was

found to be quite important that the free carrier screening be treated dynamically.

An important finding of the present investigation is that the mobility increase at low excitation levels is highly sensitive to the degree of compensation present in the material. Since the lack of thermal freezeout prevents a determination of N_A from the temperature-dependent Hall data, the present technique is quite promising as a means of accurately determining acceptor densities in narrow-gap n-type semiconductors.

ACKNOWLEDGMENTS

This work was supported in part by the Office of Naval Research and Defense Advance Research Projects Agency.

APPENDIX A: KANE BAND MODEL

In the Kane four-band model, the exact dispersion relations $k_i(E)$ for the conduction band and three valence bands are solutions to the equations[17]

$$E' = 0, \tag{A1a}$$

$$E'(E'-E_g)(E'+\Delta) - \frac{\hbar^2 k^2 E_p}{2m_0}(E' + \tfrac{2}{3}\Delta) = 0. \tag{A1b}$$

Here $E' = E - \hbar^2 k^2/2m_0$, E is referenced to the top of the valence bands, E_g is the band gap, Δ is the spin-orbit splitting, and $E_p \equiv 2m_0 P^2/\hbar^2$, where P is the $\vec{k}\cdot\vec{p}$ interaction matrix element. Equation (A1a) has the trivial solution $\hbar^2 k_h^2/2m_0 = E$, which represents the dispersion for the heavy-hole band. Equation (A1b) is cubic, however, and the analytic solutions are complicated. For both the electron and light-hole bands it is more reasonable to expand in powers of E/E_g:

$$\frac{\hbar^2 k_i^2}{2m_i} = E\left[1 + \alpha_i \frac{E}{E_g} + \beta_i \left[\frac{E}{E_g}\right]^2 + \cdots\right], \tag{A2}$$

where m_i is the effective mass at $k = 0$ and the energies have been redefined as specified below. This expression can also be used for the heavy-hole band if we set $\alpha_h = \beta_h = 0$.

After redefining $E \to E - E_g$, one obtains for electrons

$$\alpha_e = \frac{(1-\gamma_e)^2(\frac{3}{2} + 2\delta + \delta^2)}{(\frac{3}{2}+\delta)(1+\delta)} \tag{A3a}$$

and

$$\beta_e = \frac{-2(1-\gamma_e)^3}{(\frac{3}{2}+\delta)^2(1+\delta)} \times \left[\frac{1}{4}\delta^2 + \frac{\gamma_e(\frac{3}{2}+2\delta+\delta^2)^2}{(1+\delta)}\right]. \tag{A3b}$$

Here $\delta \equiv \Delta/E_g$ and

$$\gamma_e \equiv \frac{m_e}{m_0} = \left[1 + \frac{1}{3}E_p\left[\frac{2}{E_g} + \frac{1}{E_g+\Delta}\right]\right]^{-1}. \tag{A4}$$

In the present calculation we will ignore the terms of Eq. (A2) in $(E/E_g)^2$ and higher. This is always allowable for energies comparable to or less than the gap because with small γ_e, $\beta_e \lesssim 0.06$ for any δ. In $Hg_{0.8}Cd_{0.2}Te$ at 10 K, $\delta \approx 16$ which gives $\beta_e \approx 0.02$ and $\alpha_e \approx 0.97$. While most previous authors have used the reasonable approximation $\alpha_e = 1$, a few[45] have employed the more general form given by Eq. (A3a). However, Eq. (A3b) for β_e has apparently not appeared before.

For the light-hole band we redefine $E \to -E$. One then obtains

$$\alpha_l = (1+\gamma_l)^2(1+\tfrac{1}{2}\delta^{-1}), \tag{A5a}$$

and

$$\beta_l = (1+\gamma_l)^3[\tfrac{1}{2}\delta^{-1} + \tfrac{3}{4}\delta^{-2} + 2\gamma_l(1+\tfrac{1}{2}\delta^{-1})^2], \tag{A5b}$$

where

$$\gamma_l \equiv \frac{m_l}{m_0} = \frac{(\delta+\frac{3}{2})\gamma_e}{\delta + 1 - \gamma_e(2\delta+\frac{5}{2})}. \tag{A6}$$

As long as $\delta \gg 1$, the electron and light-hole masses for $k = 0$ are nearly equal. However, if $\delta \ll 1$ the light holes are heavier by a factor of about $\frac{3}{2}$, and the expansion in powers of (E/E_g) in Eq. (A2) does not converge except at extremely small energies. This is not surprising since for $\delta \ll 1$ the light hole and splitoff bands are strongly coupled.

From the truncated form of Eq. (A2), one easily obtains the useful quantity

$$\frac{dk_i}{dE} = \left[\frac{m_i}{2\hbar^2 E}\right]^{1/2} \frac{(1+2\alpha_i E/E_g)}{(1+\alpha_i E/E_g)^{1/2}}. \tag{A7}$$

The density of a particular carrier type i can be obtained as a function of its quasi-Fermi energy E_{Fi} from the relation

$$n_i = \frac{1}{\pi^2}\int_0^\infty f_0(E_{Fi})k_i^2(E)dk_i. \tag{A8}$$

In order that the screening length can be calculated one also needs the quantity

$$\frac{dn_i}{dE_{Fi}} = \frac{1}{\pi^2}\int_0^\infty \frac{\partial f_0}{\partial E_{Fi}} k_i^2(E)dk_i. \quad (A9)$$

APPENDIX B: BREAKDOWN OF BORN APPROXIMATION AND NONPARABOLICITY EFFECTS

It is shown in Ref. 21 that the Born approximation is valid as long as

$$y_e \equiv \tfrac{1}{2} k_e a_{0e} = \frac{k_e \hbar^2 \epsilon_0}{2m_e |Z_I| e^2} \gg 1. \quad (B1)$$

For very low-energy electrons this relation does not hold and it is necessary to use the phase-shift method to find the ionized-impurity scattering cross sections.

Nonparabolicity effects are important at electron energies comparable to or greater than E_g. The energy gap is related to the effective mass by Eq. (A4) which can be simplified to yield the approximate expression $E_g \approx (\frac{2}{3})E_p m_e/m_0$. If we consider the conduction band nonparabolicity to be significant when $E/E_g \geq 0.1$ [see Eq. (A2)] and the Born approximation to break down when $y \lesssim 1$, we see that both effects are important when

$$0.067\, E_p \frac{m_e}{m_0} \lesssim E \lesssim \frac{2m_e Z_I^2 e^4}{\hbar^2 \epsilon_0^2}. \quad (B2)$$

This relation is only possible if

$$\epsilon_0 \lesssim 6.4\, Z_I (E_p/20 \text{ eV})^{-1/2}. \quad (B3)$$

Since E_p is on the order of 20 eV for all of the common III-V and II-VI semiconductors while ϵ_0 is within a factor of two of 16, inequality (B3) is at most marginally satisfied even for $Z_I > 1$. Thus, any electron whose energy is sufficiently small to invalidate the Born approximation is close enough to the bottom of the conduction band to have a nearly parabolic dispersion. We conclude that accurate results can always be obtained by calculating phase-shift corrections to the Born approximation within the parabolic formalism. We have verified this by comparing with results obtained from a nonparabolic phase shift calculation.[22]

APPENDIX C: INELASTICITY OF THE ELECTRON-HOLE COLLISIONS

In this Appendix we estimate the inelasticity of the electron-hole interactions. We assume $m_h \gg m_e$ and ignore the nonparabolicity of the conduction band.

Consider an electron and hole with initial wave vectors $\vec{k}_e$ and $\vec{k}_h$ which are scattered to the final states $\vec{k}_e - \vec{q}$ and $\vec{k}_h + \vec{q}$. From conservation of energy and momentum one obtains the relation

$$q\left[\frac{1}{m_e} + \frac{1}{m_h}\right] \approx \frac{q}{m_e} = \frac{2k_e\cos\theta_e}{m_e} - \frac{2k_h\cos\theta_h}{m_h}, \quad (C1)$$

where θ_e and θ_h are the angles of $\vec{q}$ with respect to $\vec{k}_e$ and $\vec{k}_h$. Using this relation we can write

$$\frac{\Delta E_e}{E_e} = \frac{|\vec{k}_e - \vec{q}|^2 - k_e^2}{k_e^2} = \frac{q^2}{k_e^2} - \frac{2q}{k_e}\cos\theta_e$$
$$= -4\left[\frac{k_h m_e}{k_e m_h}\right]\cos\theta_h \left[\cos\theta_e - \left[\frac{k_h}{k_e}\frac{m_e}{m_h}\right]\cos\theta_h\right], \quad (C2)$$

where the second term in brackets can be ignored since $k_h m_e/k_e m_h \ll 1$. The same argument can be used in Eq. (C1) to give $\cos\theta_e \approx q/2k_e$. In the transport calculations, one integrates over q to find the momentum-transfer scattering cross section. For elastic scattering from a screened Coulomb potential in the Born approximation, the dominant region of this integral occurs in the neighborhood of some value $q_0 \approx [2/(1+\frac{1}{2}b_e^{1/2})]^{1/2}k_e$ (see Appendix D). Using this relation, the typical inelasticity can be approximated by

$$\frac{|\Delta E_e|}{E_e} \approx \frac{2^{5/2}}{\pi(1+\frac{1}{2}b_e^{1/2})^{1/2}}\left[\frac{m_e}{m_h}\frac{E_h}{E_e}\right]^{1/2} \ll 1, \quad (C3)$$

where we have used the average value $|\cos\theta_h| \approx 2/\pi$. (Since q is insensitive to θ_h, its value may be considered random.) Equation (C3) shows that $|\Delta E_e|$ may always be assumed small relative to E_e. Nevertheless, a neglect of inelasticity may cause error in mobility calculations when the

electrons are degenerate. In the more general transport theory which accounts for inelastic collisions (see, e.g., Ref. 46), one obtains an integration over final electron energies E_e' where the integrand contains a factor $[1 - f_0(E_e')]$ instead of the usual $[1 - f_0(E_e)]$ term for elastic collisions. By relaxing the requirement that $\Delta E_e = 0$, the inelastic theory may permit many more transitions and can lead to a lower electron mobility. As an example, if ΔE_e is many times $k_B T$, then initial electron states many $k_B T$ below the Fermi level can couple to unoccupied final states above the Fermi level. Therefore, the relaxation time approximation which assumes the collisions to be elastic is not expected to be accurate for degenerate electrons unless $|\Delta E_e|/k_B T \lesssim 1$. For degenerate electrons and nondegenerate holes this criterion can be written

$$\frac{|\Delta E_e|}{k_B T} \approx \frac{2^{5/2}}{\pi(1+\frac{1}{2}b_e^{1/2})^{1/2}} \times \left[\frac{3m_e}{2m_h}\frac{E_{F_e}}{k_B T}\right]^{1/2} \lesssim 1 \quad \text{(C4)}$$

which is not satisfied at high electron densities. For $Hg_{0.8}Cd_{0.2}Te$ at 10 K this occurs when $n \gtrsim 10^{17}\ \text{cm}^{-3}$.

APPENDIX D: ESTIMATE OF INTERACTION DISTANCE r_0

From the integration over scattering angles in the static Born approximation [Eq. (2.21)], one can estimate the angles $\theta \approx \theta_0$ which give the dominant contribution to the integral for any given value of b_e. Assuming parabolic bands, i.e., $O(\cos\theta) \rightarrow 1$, θ_0 can be defined by the equation

$$\int_0^{\theta_0} \frac{(1-\cos\theta)\sin\theta d\theta}{(1-\cos\theta+2/b_e)^2} = \int_{\theta_0}^{\pi} \frac{(1-\cos\theta)\sin\theta d\theta}{(1-\cos\theta+2/b_e)^2}. \quad \text{(D1)}$$

Defining $q_0^2 = 2k_e^2(1-\cos\theta_0)$, one obtains $q_0 \approx 2^{1/2} k_e$ at small b_e and $q_0 \approx 2k_e(e/b_e)^{1/4}$ in the limit of large b_e. The two results can be combined to give

$$q_0 \approx \left[\frac{2}{1+\frac{1}{2}b_e^{1/2}}\right]^{1/2} k_e, \quad \text{(D2)}$$

where for simplicity we have omitted the exponential function e. The dominant contribution to the scattering thus occurs for wave vectors on the order of q_0. The inverse of q_0 defines an average interaction distance r_0 over which the most important interactions occur. This follows since in Fourier transforming the potential $U(r)$ to obtain $U(q_0)$, the dominant contribution occurs in the region $r_0 \approx q_0^{-1}$.

Conceptually, it may seem natural to estimate the interaction distance as being comparable to the screening radius. However, the r_0 we obtain is not necessarily on the order of λ_s for the following reasons. When $b_e = 4k_e^2\lambda_s^2 \ll 1$, the above arguments show that $r_0 \gg \lambda_s$. This is reasonable because r_0 cannot be smaller than the uncertainty of the electron's position, approximately $1/k_e$. (In fact, the screened Coulomb potential is not expected to work well in this region because the electrons cannot screen effectively on a distance scale much shorter than their wavelength.) When $b_e \gg 1$, the scattering for $r < \lambda_s$ is much more effective than that for $r \approx \lambda_s$. Hence small impact parameters are emphasized and $r_0 \lesssim \lambda_s$. While a more accurate estimate of r_0 can be obtained using phase-shift techniques,[39] such refinements are not required here.

[1]D. Long, Phys. Rev. 176, 923 (1968).

[2]C. T. Elliott and I. L. Spain, Solid State Commun. 8, 2063 (1970).

[3]S. Otmezguine, F. Raymond, G. Weill, and C. Vérié, in *Proceedings of the Tenth International Conference on the Physics of Semiconductors, Cambridge, 1970,* edited by S. P. Keller, J. C. Hensel, and F. Stern [Nat. Bur. Stand (U.S.), Springfield, Va., 1970], p. 536.

[4]B. L. Gel'mont, V.I. Ivanov-Omskii, B. T. Kolomiets, V. K. Ogorodnikov, and K. P. Smekalova, Fiz. Tekh. Poluprovdn. 5, 266 (1971) [Sov. Phys.— Semicond. 5, 228 (1971)].

[5]J. Stankiewicz and W. Giriat, Phys. Status Solidi B 48, 467 (1971).

[6]W. Scott, J. Appl. Phys. 43, 1055 (1972).

[7]G. Nimtz, G. Bauer, R. Dornhaus, and K. H. Müller, Phys. Rev. B 10, 3302 (1974).

[8]J. J. Dubowski, Phys. Status Solidi B 85, 663 (1978).

[9]F. J. Bartoli, R. E. Allen, L. Esterowitz, and M. R. Kruer, Solid State Commun. 25, 963 (1978).

[10]J. R. Meyer and F. J. Bartoli (unpublished).

[11]H. Ehrenreich, J. Phys. Chem. Solids 2, 131 (1957); 9, 129 (1959).

[12]T. C. Harman and J. M. Honig, J. Phys. Chem. Solids 23, 913 (1962).

[13]W. Zawadzki and W. Szymanska, Phys. Status Solidi B 45, 415 (1971).

[14]D. L. Rode, in *Semiconductors and Semimetals,* edited by R. K. Willardson and A. C. Beer (Academic, New York, 1975), p.1.

[15]D. Chattopadhyay and B. R. Nag, Phys. Rev. B 12, 5676 (1975).

[16]D. A. Nelson, J. G. Broerman, C. J. Summers, and C. R. Whitsett, Phys. Rev. B 18, 1658 (1978).

[17]E. O. Kane, J. Phys. Chem. Solids 1, 249 (1957).

[18]F. J. Blatt, J. Phys. Chem. Solids 1, 262 (1957).

[19]J. B. Krieger and S. Strauss, Phys. Rev. 169, 674 (1968).

[20]A. D. Boardman and D. W. Henry, Phys. Status Solidi B 60, 633 (1973).

[21]J. R. Meyer and F. J. Bartoli, Phys. Rev. B 23, 5413 (1981).

[22]J. R. Meyer and F. J. Bartoli (unpublished).

[23]F. Stern, Phys. Rev. 148, 186 (1966).

[24]F. Stern, Phys. Rev. 158, 697 (1967).

[25]Although the assertions are somewhat better in the higher-temperature intrinsic regime which was of primary interest to the authors of Refs. 11, 13, 14, and 16, some error is also introduced in that region.

[26]D. L. Carter, M. A. Kinch, and D. D. Buss, in *The Physics of Semimetals and Narrow Gap Semiconductors,* edited by D. L. Carter and R. T. Bate (Pergamon, Oxford, 1971), p. 273.

[27]J. Lindhard, K. Dan. Vidensk. Selsk. Mat.-Fys. Medd. 28, No. 8 (1954).

[28]S. Perkowitz and R. H. Thorland, Solid State Commun. 16, 1093 (1975).

[29]J. M. Ziman, *Principles of the Theory of Solids,* 2nd ed. (Cambridge University Press, Cambridge, 1972), p. 164.

[30]The "appropriate" hole velocity $\bar{v}_h$ is somewhat lower than the average value since in Eq. (2.19), the usual density-of-states factor v_h^2 is absent. One might therefore define $\bar{v}_h = \langle v_h^{-2} \rangle^{-1/2} \rightarrow (k_B T/m_h)^{1/2} (p/p')^{1/2}$, where p' is defined in Eq. (2.20).

[31]W. Scott, E. L. Stelzer, and R. J. Hager, J. Appl. Phys. 47, 1408 (1976).

[32]O. Caporalett and W. F. Mickelthwaite, Bull. Am. Phys. Soc. 26, 423 (1981).

[33]B. Schlicht, A. Alpsancar, G. Nimtz, and A.N.F. Schroeder, in Proceedings of the Fourth International Conference on the Physics of Narrow Gap Semiconductors, Lintz, 1981 [Lect. Notes Phys. 152, 439 (1982)].

[34]H. Brooks (unpublished). See L. Makowski and M. Glicksman, J. Phys. Chem. Solids 34, 487 (1973).

[35]J. Kossut, Phys. Status Solidi B 86, 593 (1978).

[36]Equation (2.19) contains an explicit factor $k_e^{-2} dk_e/dE_e$. From the static result Eq. (2.4) there is also a factor of approximately p', the effective density of hole-scattering centers. This is at most (for nondegenerate holes and degenerate electrons) $p' \approx p \approx n \sim k_e^3$. The total increase of τ_{eh}^{-1} with n is therefore no greater than $k_e dk_e/dE_e$. There is also a screening factor [F_I in Eq. (2.20)] which usually decreases somewhat with n_e, although under certain conditions it can increase slightly.

[37]H. R. Vydyanath, J. Vac. Soc. (in press).

[38]J. R. Meyer and F. J. Bartoli (unpublished).

[39]J. R. Meyer and F. J. Bartoli, J. Phys. C 15, 1987 (1982). An application of the criterion discussed in this paper shows that multi-ion-scattering effects may be neglected in uncompensated nonphotoexcited $Hg_{1-x}Cd_xTe$. However, the validity of the single-site model may be somewhat marginal in more compensated material. Unfortunately, there is presently no reliable theory available for taking multi-ion effects into account. Because of the increased screening by free carriers, multi-ion effects are generally unimportant under conditions of photoexcitation, even when the degree of compensation is fairly high. One may also ignore events in which an electron scatters from more than one photoexcited hole at the same time.

[40]H. Brooks, Adv. Electron. Electron Phys. 7, 85 (1955).

[41]M. Lax, Phys. Rev. 119, 1502 (1960).

[42]B. V. Kornilov and S. E. Gorskii, Fiz. Tekh. Poluprovdn. 2, 262 (1968) [Sov. Phys.—Semicond. 2, 216 (1968)].

[43]R. L. Petritz, Phys. Rev. 110, 1254 (1958).

[44]J. R. Meyer, Phys. Rev. B 21, 1554 (1980).

[45]E. D. Palik, G. S. Picus, S. Teitler, and R. F. Wallis, Phys. Rev. 122, 475 (1961).

[46]J. R. Meyer and F. J. Bartoli, Phys. Rev. B 24, 2089 (1981).